Surfaces and Interfaces 46 (2024) 104006

Contents lists available at ScienceDirect

Surfaces and Interfaces

journal homepage: www.sciencedirect.com/journal/surfaces-and-interfaces

Two-dimensional periodic surface nanotexturing of 6H-SiC by ultrashort laser pulses

M. Mastellone [a,*], E. Bolli [b], V. Valentini [b], A. Bellucci [b,*], S. Orlando [a], A. Santagata [a], R. Polini [c], A. Lettino [d], E. Sani [e], D.M. Trucchi [b]

[a] Istituto di Struttura della Materia (ISM-CNR), Consiglio Nazionale delle Ricerche, Sede Secondaria di Tito Scalo, Area Industriale - Contrada S. Loia, 85050 Tito Scalo, Potenza, Italy
[b] Istituto di Struttura della Materia (ISM-CNR), Consiglio Nazionale delle Ricerche, DiaTHEMA Lab, Sede Secondaria di Montelibretti, Via Salaria km 29.300, 00015 Monterotondo Stazione, Roma, Italy
[c] Università di Roma "Tor Vergata", Dipartimento di Scienze e Tecnologie Chimiche, Via della Ricerca Scientifica 1, 00133 Roma, Italy
[d] Istituto di Metodologie per l'Analisi Ambientale (IMAA-CNR), Consiglio Nazionale delle Ricerche, Area Industriale - Contrada S. Loia, 85050 Tito Scalo, Potenza, Italy
[e] Istituto Nazionale di Ottica (INO-CNR), Consiglio Nazionale delle Ricerche, Largo E. Fermi, 6, I-50125 Firenze, Italy

ARTICLE INFO

Keywords:
Laser texturing
Silicon carbide
LIPSS
Surface functionalization
Cold processing

ABSTRACT

Circularly polarized femtosecond laser pulses have successfully promoted the formation of Two-Dimensional Laser Induced Periodic Surface Structures (2D-LIPSS) exhibiting a sub-wavelength periodicity of 150 ± 20 nm on semi-insulating 6H-SiC samples. The main objective of this study was to discern the formation of two-dimensional LIPSS depending on the single pulse energy and the number of pulses released per unit area. The experimental laser system used in this study generates pulses with a duration of 100 fs, a wavelength of 800 nm, and operates at a repetition rate of 1 kHz.

Micro-Raman spectroscopy confirms the presence of the characteristic 6H-SiC peaks across all irradiated samples, indicating that the processing technique does not induce significant compositional variations. Nonetheless, the analysis reveals the induction of compressive stress within the lattice structure.

Samples treated across the entire surface were characterized by using optical analysis in order to assess the induced variations in absorptance and emittance due to laser irradiation. The treated samples exhibit solar absorptance values of approximately 75 % and a high spectral selectivity up to 2.0 for temperatures higher than 1000 K. This highlights the potential of fs-laser surface textured 6H-SiC plates as viable selective solar absorbers for energy conversion devices operating at elevated temperatures.

1. Introduction

The use of ultrashort laser pulses for cold-processing materials has emerged as a versatile and promising technique with significant advantages in tailoring and enhancing various physical and chemical properties [1]. By employing ultrafast laser pulses with durations in the femtosecond range, precise manipulation of materials at the microscale [2] and nanoscale [3] is achieved while minimizing the undesired effects of heat accumulation [4]. This innovative approach enables the properties customization and enhancement of a wide range of materials, leading to advancements in diverse fields including solar energy harvesting [5,6]. Indeed, the achievement of functional surfaces with enhanced solar absorption properties is of utmost importance for the fabrication of performing selective absorbers. In the past, fs-laser treatments have been performed on engineered ultra-high temperature ceramics, such as HfC [7], TaC, [8] and TaB_2 [9], and refractory metals such as molybdenum [10] for the capture of the concentrated sunlight.

A key phenomenon that has garnered significant attention for the tailoring of the optical properties of treated materials is the formation of Laser-Induced Periodic Surface Structures (LIPSS) [11]. LIPSS are nanoscale patterns that appear on the material surface during the interaction with ultra-short laser pulses and facilitates surface modifications with remarkable control on geometry [12] and spatial resolution [13], surpassing the limitations of traditional optical technologies. Among many applications, LIPSS have demonstrated potential in manipulating mechanical [14] and optical properties [15,16],

* Corresponding author.
E-mail addresses: matteo.mastellone@ism.cnr.it (M. Mastellone), alessandro.bellucci@cnr.it (A. Bellucci).

https://doi.org/10.1016/j.surfin.2024.104006
Received 6 September 2023; Received in revised form 18 January 2024; Accepted 27 January 2024
Available online 28 January 2024

fine-tuning of surface wettability [17], electrochemical properties [18], interaction with THz radiation [19] and lastly even influencing biological interactions [20,21].

The formation of LIPSS is governed by various physical phenomena that are closely correlated to the properties of the irradiated materials. In the case of highly absorptive materials like metals, the prevailing theory suggests that LIPSS derive from the interference between the incident laser wave and the waves scattered or excited at the material's surface [22], such as surface plasmon polaritons [23]. This interference modulation can lead to localized ablation and the formation of regularly spaced ripples when the incident light is linearly polarized. On the other hand, the origin of LIPSS in low-absorption materials such as wide bandgap semiconductors is still a subject of debate [24]. Several mechanisms have been proposed, including second harmonic generation (SHG) [25], interference between the laser beam and surface plasmon polaritons (SPPs) [26], surface relaxation through self-organization [27], and Coulomb explosion [28]. However, the most widely accepted theory for LIPSS formation on dielectric materials suggests that they arise from the coherent superposition of the scattered near-field at the surface and the incident electromagnetic field generated by the propagating laser beam [29,30].

The understanding and control of LIPSS formation mechanisms hold paramount importance in the field of nanoscale surface engineering of several promising materials for different opto-electronic applications (e.g., [31]). Among them, silicon carbide (SiC) has garnered significant attention due to its exceptional properties [32], making it an ideal material for optical [33] and electronic applications [34]. With its wide bandgap, high thermal conductivity and excellent mechanical strength, SiC exhibits remarkable potential for the fabrication of photonic devices, but is limited in the interaction with the visible radiation [35]. Therefore, to fully capitalize on these advantages, effective strategies for enhancing absorption in the visible range for SiC are essential as proved by the many efforts carried out in this direction [36–39].

In this paper, we present a comprehensive study aimed at assessing the effectiveness of two-dimensional Laser-Induced Periodic Surface Structures (2D-LIPSS) in enhancing solar absorption properties of silicon carbide (SiC) on wide surface areas. Whereas photovoltaics involves active materials that operate at temperatures close to room temperature, the design of thermal solar absorbers serves a different purpose. These absorbers are intentionally engineered to reach and operate at elevated temperatures, even exceeding 1000 °C. To this end, optical absorption must be maximized. Conversely, at high temperatures, thermal radiation represents a potential energy loss to be minimized. To fulfil these distinct requirements, simple and more robust absorbers are developed, featuring bulk materials with engineered textured surfaces. This approach ensures enhanced stability and durability, critical attributes for meeting the demands of these challenging high-temperature applications.

Building upon previous experiments [13,35], we propose to fabricate 2D-LIPSS on 6H-SiC in one single irradiation step by using circular polarization to induce a geometrical enhancement for the light trapping. Recently, it has been demonstrated that it is possible to obtain array of nanocolumns on 4H-SiC by using a two-step laser-inducing method [40]. By systematically varying the number of pulses and single pulse energy, we investigate the occurrence of 2D-LIPSS on SiC surfaces to improve their efficiency as selective solar absorbers, paving the way for advancements in photonic and energy conversion devices. Through detailed physico-chemical characterization using Raman spectroscopy, we ensure the absence of undesired chemical or structural alterations, while, through optical analysis, we seek to provide a deeper understanding of the potential of 2D-LIPSS in enhancing solar absorption properties of SiC further validating the viability of this approach. Furthermore, the process scanning mode demonstrated its efficacy in uniformly treating large silicon carbide areas, yielding significant improvements in the functional surface properties. This research not only contributes to fundamental knowledge but also holds practical implications for harnessing enhanced optical properties in applications ranging from energy conversion to photonics.

2. Materials and methods

2.1. Laser texturing

The surface nanotexturing treatments were performed using a Ti:Sapphire femtosecond laser (Spectra-Physics, Milpitas, CA, USA) with the following characteristics: 100 fs pulse duration, linear polarization, wavelength $\lambda_{fs} = 800$ nm, adjustable repetition rate up to 1 kHz. The laser beam was generated by a mode-locked oscillator and subsequently regeneratively amplified. The pulses outcoming from the laser system were linearly polarized, so a rotation at 45° to the optic axis of a λ/4 plate was used to turn the polarization to circular.

Pulses were perpendicularly focused in air by an objective lens (4×, N.A. = 0.10) onto the surface of a commercially available 6H-SiC (10 × 10 × 0.5 mm^3, double-side polished, roughness < 30 nm, provided by Precision Micro-Optics Inc.). As a first approximation, the laser spot-size was assessed *a posteriori* by analysing the ablation and modification areas with scanning electron microscopy (SEM).

After the laser irradiation, a cleaning process was applied by immersing the samples in an ultrasonic bath with acetone for 10 min and rinsing them in deionized water to remove nano-debris.

2.2. Structure and morphology characterization

Surface morphology was analysed by Field-Emission Gun Scanning Electron Microscopy (FEG SEM) obtained by a Zeiss Microscope (model Leo Supra 35; Oberkochen, Germany).

The software Gwyddion (version 2.62) was used to perform 2D Fast Fourier Trans-formation (2D-FFT) analysis of 30 × 30 μm^2 sized SEM images to obtain reliable values of LIPSS periodicity.

2.3. Physico-chemical characterization

Physico-chemical characterization was carried out by Raman spectroscopy using a Horiba Scientific LabRam HR Evolution confocal spectrometer equipped with a 100 mW Oxxius ($\lambda_{exc} = 532$ nm) laser source and a computerized XY-table, an electron-multiplier CCD detector, and an Olympus U5RE2 microscope with a 100x objective (laser spot on the sample surface 0.7 μm) with a numerical aperture (NA) of 0.9, and a grating with 1800 grooves/mm were used. All Raman spectra were recorded in backscattering geometry focalizing 10 % of the laser source power at the sample and twenty spectra with an accumulation time of 10 s were averaged. Samples were measured from 100 to 1800 nm.

2.4. Optical characterizations

The optical behaviour of nanotextured 6H-SiC samples was determined at room temperature through optical transmittance and hemispherical reflectance measurements in two wavelength ranges: (1) 0.30–2.5 μm, by using a double-beam spectrophotometer (Perkin Elmer "Lambda900", MA, USA) equipped with a 150 mm diameter Spectralon®-coated integration sphere; (2) 2.5–11.0 μm by means of a Fourier Transform spectrophotometer (FT-IR Bio-Rad "Excalibur", CA, USA) equipped with a gold-coated integrating sphere and a liquid nitrogen-cooled detector. In all the cases, the spectra were acquired for a quasi-normal incidence angle.

3. Results and discussion

In this section, we present a comprehensive analysis of the morphological and structural properties of the irradiated samples. Our study focuses on the direct irradiation of single spots on the surfaces of

6H-SiC, i.e., absence of any relative movement between sample and laser beam. The first objective was to investigate the effects of the laser treatments on the resulting morphological and physico-chemical characteristics, specifically as a function of the number of pulses, N, and pulse energy, E_P. The pulse fluence, Φ, is equal to $\Phi = E_P/(\pi r^2)$, where r is the $1/e^2$ Gaussian beam radius of the circular spot.

Table 1 provides a detailed summary of the experimental parameters employed for the treatments under investigation. After conducting preliminary irradiations at high pulse energies, which led to severe damage even with a low number of pulses (<10), we adopted a strategy that involved selecting a set of four pulse energy levels. The selected pulse energies were carefully calibrated to work above the threshold for the LIPSS fabrication, while also avoiding the occurrence of extensive damage. Additionally, for each pulse energy level, we conducted a series of experiments employing different numbers of impinging pulses, and thus obtained different values of accumulated pulse fluence, defined as $\Phi_{acc} = N \bullet \Phi$. For the sake of completeness, the conditions that did not result in a successful LIPSS fabrication are also reported in the table.

The plot presented in Fig. 1a graphically shows the two regions for which it was possible to observe or not the formation of LIPSS as a function of treatment parameters, with a narrow region that will be investigated in the future for which the LIPSS formation is not assured. A prominent observation from Fig. 1a is the evident decrease in the number of pulses required for LIPSS formation as the energy per pulse increases. McDaniel et al. elucidated this phenomenon in Ref. [41], proposing that the lowered threshold fluence needed can be attributed largely to alterations in the average surface reflectivity that decreases due to laser induced damage (i.e., the incubation parameter is strictly correlated to the surface reflectivity). This implies that damaging the material becomes easier at higher pulse energies. Additional studies on the role of surface roughness [36] and surface defects [42] on the decreasing energy threshold needed for LIPSS formation confirm this hypothesis.

Through this systematic approach, our analysis seeks to provide a comprehensive understanding of the morphological and structural changes induced by laser treatments, to elucidate the underlying mechanisms and establish correlations between these parameters and the observed alterations.

3.1. Morphological analysis of irradiated spots

First, preliminary SEM investigations were performed to calculate the $1/e^2$ Gaussian beam diameter, w, of the circular spot on the focal plane. Using the method proposed by Liu [43], the diameter was estimated to be approximately 36 ± 4 μm. All the SEM images presented in this study were captured at the center of the laser spot. It is important to note that, due to the Gaussian irradiance distribution of the laser beam, the periphery of the spot receives lower energy intensity, falling below the modification threshold required for LIPSS fabrication. However, in practical applications, laser treatments are typically performed over larger areas, rather than on individual spots. In such cases, this undesired effect becomes negligible as the superimposition of multiple laser pulses during translational movements ensures that the below-threshold regions are effectively covered, eliminating the presence of low accumulated fluence borders [44,45]. Therefore, this effect is not critical when considering the overall treatment area and its impact on the desired surface modifications if a uniform energy distribution is obtained [44].

Fig. 1b shows how the circularly polarized irradiation induced the formation of a two-dimensional patterning extending fully over the sample irradiated area. This can be described as formed by anisotropically distributed nano-bumps with a circular shape, and presenting an equivalent diameter of approximately 85 nm, which is well below the laser wavelength used during the experiment. The observed two-dimensional patterning was already demonstrated in Ref.[46] by Durbach et al. on a gold thin film deposited on a silicon wafer and it was attributed to a self-organization process driven by feedback-loop of interfering surface plasmon polaritons.

Another interesting observation that can be drawn out from Fig. 1c–e is that the homogeneity of such structures degrades as the single pulse energy increases. A higher pulse energy leads to a loss of the spatial order distribution of the nanostructures, but also induces melting and redeposition phenomena. This trend suggests that more consistent structures are obtained when lower pulse energies are used, as it is evidenced in Fig. 1f for the A3 sample. It is also worth noting that analogous results to A3 were obtained for a number of pulses between 583 and 700 with the energy pulses fixed at 70 μJ (Φ = 7.3 J cm^{-2}).

The 2D-FFT analysis (shown in Fig. 1g) points out the presence of distinct bright spots, indicating the occurrence of a unique spatial periodicity of about 150 ± 20 nm and a fairly ordered arrangement, which is only detected for the samples produced at the lowest single pulse energy of approximately 70 μJ (Φ = 7.3 J cm^{-2}). The spatial periodicity is in agreement with the theory that ascribes its origin to the second harmonic generation of electromagnetic fields on the sample surface [25]. The theoretical value is in this case equal to $\Lambda = \lambda_{fs}/2n$ = 153 nm, where n = 2.614 is the refractive index of the SiC sample measured at 800 nm [47]. Since the spacing between adjacent structures is lower than $\lambda_{fs}/5$, the structures formed can be classified as HSFL (High-Spatial Frequency LIPSS).

For the sake of brevity, we only show the SEM micrographs for the samples B3 to provide an example on the obtained results (Fig. 1h). The 2D-FFT transformation (Fig. 1i) shows absence of distinct bright spots, substituted by a ring, indicating a broader distribution of spatial periods. However, even in this case, a maximum intensity around the spatial periodicity of 6.53 μm^{-1} is identified, corresponding to Λ = 153 ± 30 nm. It is important to highlight that all the samples that were irradiated with a single pulse energy greater than 70 μJ present a 2D-FFT similar to the one presented in Fig. 1i, thus confirming that the most regular structures are obtainable for the lowest employed energy pulse.

Table 1
Experimental parameters of the different laser irradiation treatments. The table reports the values of E_P, Φ and N.

Samples	Single Pulse Energy (μJ)	Pulse fluence (J cm^{-2})	N of Pulses per spot	Notes
A1	70 ± 3.5	7.3 ± 0.7	467	No LIPSS detected
A2	70 ± 3.5	7.3 ± 0.7	583	
A3	70 ± 3.5	7.3 ± 0.7	636	
A4	70 ± 3.5	7.3 ± 0.7	700	
B1	80 ± 4	8.4 ± 0.8	70	No LIPSS detected
B2	80 ± 4	8.4 ± 0.8	140	
B3	80 ± 4	8.4 ± 0.8	280	
B4	80 ± 4	8.4 ± 0.8	467	
C1	91 ± 4.5	9.5 ± 0.9	35	No LIPSS detected
C2	91 ± 4.5	9.5 ± 0.9	70	
C3	91 ± 4.5	9.5 ± 0.9	140	
C4	91 ± 4.5	9.5 ± 0.9	350	
D1	107 ± 5	11.1 ± 1	23	No LIPSS detected
D2	107 ± 5	11.1 ± 1	35	
D3	107 ± 5	11.1 ± 1	58	
D4	107 ± 5	11.1 ± 1	175	

3.2. Physico-chemical characterization

Micro-Raman spectroscopy was employed to investigate the physico-chemical changes induced by the laser treatment. In this section, we will focus on presenting the differences observed between samples irradiated at different single pulse energies. It is important to note that there were no notable differences between samples irradiated with varying numbers of pulses at a given single pulse energy. By focusing on the

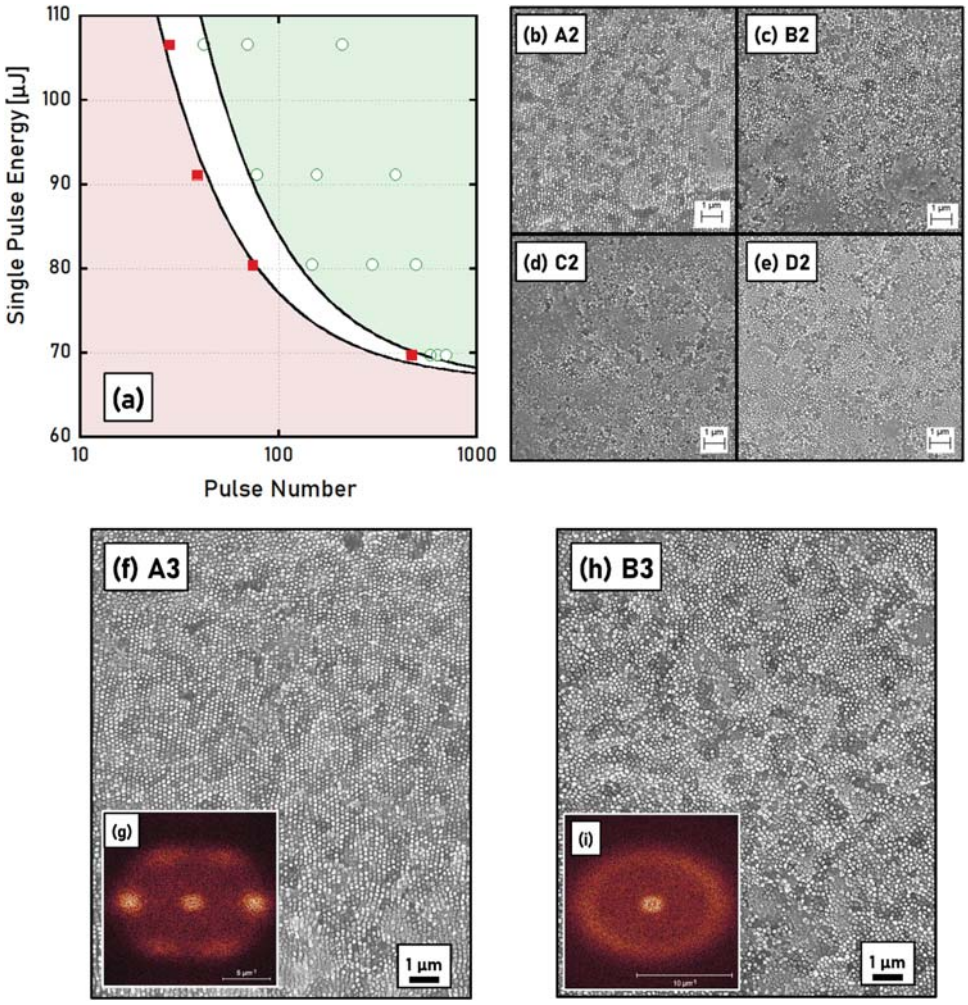

Fig. 1. (a) Parameter map (Single Pulse Energy, Pulse Number) indicating the regions where LIPSS formation occurred using a circular polarization. For the sake of clarity, single pulse fluences, calculated assuming a radius of the Gaussian beam circular section of approximately 18 ± 2 μm, are reported in Table 1. The black lines derive from the application of hyperbolic functions by fitting the NO LIPSS points, and the LIPSS points at the lowest Pulse Number. The white narrow region represents an area to be investigated to finely find the minimum fluence for the LIPSS formation according to the experimental conditions. The key for the various observations is shown as an inset. (b, c, d, e) SEM micrograph of 6H-SiC samples irradiated at four different pulse energies (A2 = 70 μJ; B2 = 80 μJ; C2 = 91 μJ; D2 = 107 μJ) at the lowest number of pulses that allowed regular nano-patterning (A2 = 583 pulses; B2 = 140 pulses; C2 = 70 pulses; D2 = 35 pulses). (f) SEM micrograph of sample A3 (E_p = 70 μJ; Φ = 7.3 J cm^{-2}; N = 636) at low magnification. In the inset (g) the 2D-FFT transformation of the SEM image is shown. (h) SEM micrograph of sample B3 (E_p = 80 μJ; Φ = 8.4 J cm^{-2}; N = 280) at low magnification. In the inset (i) the 2D-FFT transformation of the SEM image is shown.

single pulse energy variation, we can efficiently highlight alterations derived from the laser treatment and gain valuable insights into the underlying mechanisms of the observed changes.

Raman spectra of A2, B2, C2 and D2 single spots are shown in Fig. 2. The figure shows Raman spectra collected using the green wavelength (λ_{exc} = 532 nm). For every spot, the laser beam was focused on the center of the ablation crater. For the sake of comparison, the Raman spectrum of untreated 6H-SiC is reported in the same figure and labelled as reference.

All the spectra exhibit well-defined characteristic peaks of 6H-SiC, consistent with findings in existing literature [48]. Notably, the sharp peaks at 765 cm^{-1} and 787 cm^{-1} correspond to the FTO (folded transverse optic) modes, while the peak at 962 cm^{-1} relates to the FLO (folded longitudinal optic) mode. This indicates that the laser treatment effectively preserved the fundamental structure of the bulk material. Additionally, the second-order FTO and FLO signals are visible within the wave number range of 1375 to 1575 cm^{-1} and, at lower frequencies, the transverse (FTA) and longitudinal (FLA) acoustic modes (FTA at 263 cm^{-1}, FLA at 502 and 513 cm^{-1}, respectively) are evident, further confirming the absence of unwanted alterations.

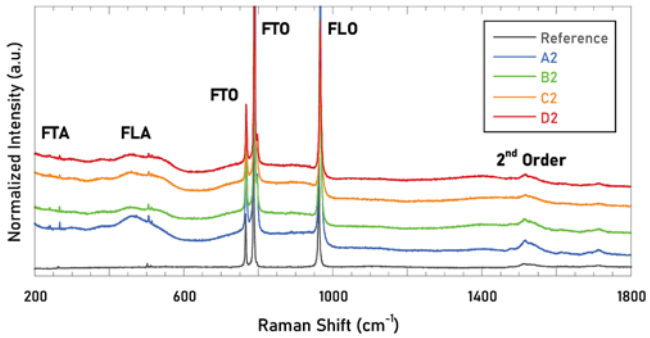

Fig. 2. Micro-Raman spectra of nanotextured 6H-SiC fabricated with different values of pulse energies (A2 = 70 μJ; B2 = 80 μJ; C2 = 91 μJ; D2 = 107 μJ). For the sake of clarity, single pulse fluences, calculated assuming a radius of the Gaussian beam circular section of approximately 18 ± 2 μm, are reported in Table 1. The most-significant features are labelled in black.

Compared to the reference SiC, the FLO signals of the four treated samples exhibit a blue shift of 3–5 cm^{-1}, and the FTO signals show a blue shift of 2 cm^{-1}, which are indicative of a slight compressive stress induced by the laser treatment. Moreover, the FWHM (full width at half maximum) of the FTO mode (3.6 cm^{-1} for the reference) widens by 1.4–3.2 cm^{-1}, and the FLO FWHM (2.6 cm^{-1} for the 787 cm^{-1} band and 2.8 cm^{-1} for the 765 cm^{-1} band in the case of the reference) also broadens by 0.8–1.5 cm^{-1} for the treated samples, due to a significant larger disorder in the lattice structure caused by the nanostructuring induced from the laser irradiation.

Conversely, the signals of the FTA and FLA modes present negligible shifts in the four treated samples spectra. Furthermore, it is possible to notice that below 600 cm^{-1} an interferential pattern overlaps the acoustic mode signals showing that the laser source generates the interference fringes as a sum of the contributes from the air/treated SiC surface and the treated SiC/bulk SiC surface.

The results obtained by SEM and Raman investigations point out that the overall SiC structure is maintained unaltered, nevertheless the laser treatment induces always a residual compressive strain in the 6H-SiC lattice. It is noteworthy to point out the absence of bands related to the formation of graphite and/or disordered carbon.

3.3. Optical characterization

To assess the impact of the laser treatment on the optical properties, we expanded the nanotexturing process to cover the entire surface of the 6H-SiC plates (size of 1 × 1 cm^2). This was achieved by employing an automated X-Y translational stage, which allowed us to perform a raster scan with 30 μm of distance between two contiguous lines along the two orthogonal directions to the laser beam propagation path. By adjusting the scanning speed, we varied the number of pulses applied per spot while keeping the pulse fluence and repetition rate constant. In essence, this approach allowed us to control the extent of laser exposure on the samples, enabling the investigation of the optical changes induced by the treatment. 6H-SiC plates were irradiated on the entire area, with the selected pulse energy and translational speed corresponded to sample A2 (Φ = 7.3 J cm^{-2}; N = 583; circular polarization; air), which is the treatment providing the most regular patterning as assessed by 2D-FFT. It is important to denote that the fabrication parameters used, in combination with the chosen distance between two contiguous lines, do not guarantee a uniform energy distribution because the optimal distance between two contiguous line to obtain a uniform value of accumulated average fluence should be < 0.45 w [44]. However, as reported in Fig. 3a, we nonetheless obtain a fairly regular nanotexturing. In Fig. 3b a macroscopic picture of the samples after irradiation on the entire area is shown. The optical characteristics of nanotextured 6H-SiC samples were assessed at room temperature by measuring spectral transmittance $T(\lambda)$ and hemispherical reflectance $R(\lambda)$. The spectral absorptance $A(\lambda)$ is subsequently derived using the relationship:

$$A(\lambda) = 1 - T(\lambda) - R(\lambda) \quad (1)$$

In Fig. 4a the absorptance spectra of the nanotextured samples in the wavelength range 0.3–11.0 μm are shown, as well as the spectra measured for the reference untreated surface (black line). The graph also displays spectra of samples investigated in our previous work [35]: 1D-LIPSS nano-texturing labelled with S1 (Φ = 1.1 J cm^{-2}; N = 1080; linear polarization; vacuum) and irregularly patterned texturing labelled with S3 (Φ = 1.1 J cm^{-2}; N = 2690; linear polarization; vacuum) in the paper of Ref [35]..

The laser-treated sample demonstrates noteworthy improvements in optical absorptance, with a pronounced enhancement observed in the visible and near-infrared (near-IR) regions, if compared to the pristine 6H-SiC plate. Of particular interest, the most prominent increase in absorptance is notably within the wavelength range spanning from 300 nm to approximately 3 μm, aligning with a significant segment of the solar spectrum. Furthermore, the absorptance profile exhibits a gradual decrease with a consistent slope extending beyond ~ 0.6 μm. This behaviour suggests favourable attributes for the material's potential role as a selective solar absorber. The observed rise in absorptance is correlated to the formation of distinct surface features. These features play a dual role, enhancing the radiation trapping and, at the same time, expanding the effective surface area available for the interaction with the incoming electromagnetic radiation. Specifically, surface structures smaller than the wavelength of light induce antireflective mechanisms through the internal reflection and the graded index layer effect, as exemplified by the documented instances of moth's eyes employing sub-wavelength structures for antireflection [49]. Conversely, structures on the surface that exceed the wavelength of light contribute to absorption by trapping light in cavities, as described by the Fresnel angular dependence of reflection [50]. In comparison to the previously investigated samples [35], the laser treatment performed in the present work presents a notable advantage: a significant lower absorptance in the mid-IR, which means a lower thermal emittance. It is also important to point out that the regular two-dimensional pattern show a higher absorptance, if compared to the regular 1D pattern, in the UV–VIS-near IR, i.e. at the wavelengths of solar spectrum.

The study aims to assess the feasibility of using laser-nanotextured 6H-SiC plates for solar applications. To gauge the effectiveness of these plates, a key parameter to be analysed is the solar absorptance (α), defined as:

$$\alpha = \frac{\int_{\lambda_1}^{\lambda_2} A(\lambda) W_{solar}(\lambda) d\lambda}{\int_{\lambda_1}^{\lambda_2} W_{solar}(\lambda) d\lambda}, \quad (2)$$

where $W_{solar}(\lambda)$ is the global-tilt GT 1.5 airmass and $A(\lambda)$ is the solar irradiance in the wavelength range between λ_1 = 300 nm and λ_2 = 3000 nm. By its definition, it immediately follows that $\alpha \leq 1$ (100 % in percentage).

As it is possible to appreciate in Fig. 4b, the two-dimensional regular patterning leads to a clear improvement in terms of solar absorptance if compared with the regular 1D-LIPSS obtained in Ref [35]., with an enhancement from 58 % to 75 %. However, the α value for 2D-LIPSS is close to that obtained for to the irregular structures (74 %). This could be attributed to a similar increase of the effective absorbing area induced by the laser radiation, but without the presence of irregular grooves and/or deep holes.

Fig. 4c shows the integrated emittances as a function of temperature for the sample prepared in the current work and the data obtained in our previous experiments (sample labelled S1 and S3 in Ref [35].). The integrated emittance (ε) is defined as:

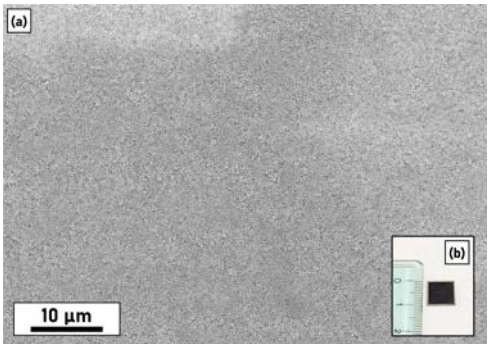

Fig. 3. (a) Large area sample fabricated with the selected pulse energy and translational speed corresponding to sample A2 (Ep = 70 μJ; Φ = 7.3 J cm^{-2}; N = 583). The laser irradiation followed a raster scan with 30 μm of distance between two contiguous lines along the two orthogonal directions to the laser beam propagation path. (b) Macroscopic picture of the sample irradiated on its entire surface after the raster scan process.

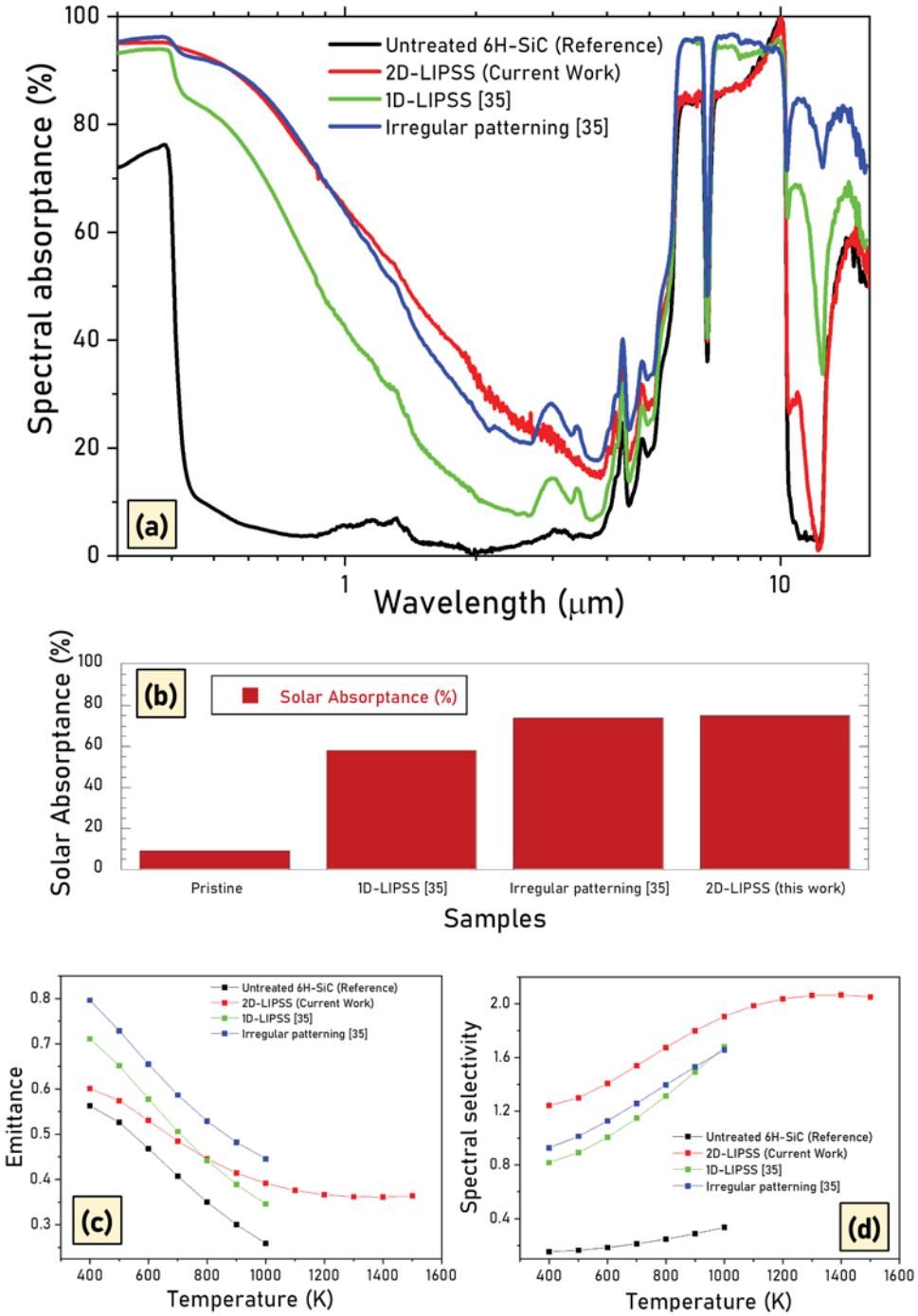

Fig. 4. (a) Absorptance spectra in the wavelength range 300 nm–11 μm, (b) Solar absorptance values calculated according to Eq. (2), (c) Integrated emittance and (d) spectral selectivity in the temperature range 400–1600 K. All the graphs are based on the results obtained after measuring the sample treated in this current work (2D-LIPSS), the samples reported in Ref.[35] and the untreated sample (also labelled as reference). The 1D-LIPSS corresponds to the sample labelled with S1 in Ref. [35] and the irregularly patterned surface corresponds to the sample labelled with S3 in Ref.[35].

$$\varepsilon = \frac{\int_{\lambda_1}^{\lambda_3} A(\lambda)B(\lambda,\ T)d\lambda}{\int_{\lambda_1}^{\lambda_3} B(\lambda,T)d\lambda} \tag{3}$$

where $B(\lambda,T)$ is the blackbody spectral radiance at the operating absorber temperature T, and spectrally integrated into between $\lambda_1 = 300$ nm and $\lambda_3 = 16$ μm wavelength range accessible by our spectrophotometric analysis.

A high thermal emittance is undesirable for selective solar absorbers as it leads to the re-emission of a substantial portion of absorbed sunlight as black-body radiation, contributing to thermal losses rather than being effectively utilized for energy conversion. This phenomenon significantly diminishes the efficiency of the absorber, and its impact becomes more pronounced with increasing temperatures. The 2D-LIPSS present a better performance, in terms of emissivity, within the range comprised between room temperature and 800 K if compared to the previous results obtained in Ref. [35]. Another interesting observation is that both regular patterned samples (2D-LIPSS, pertaining to this work, and sample S1 pertaining to Ref. [35]) display a lower emissivity, suggesting that more ordered patterns could be more suited as a selective solar absorber.

Another key parameter for evaluating the performance of a solar absorber is the spectral selectivity, also known as the α/ε ratio. A solar absorber should ideally have a low emittance to minimize thermal radiation losses. Therefore, the spectral selectivity α/ε should be as high as possible. Fig. 4d shows α/ε in the temperature range 400–1600 K. This outcome is notably promising, especially when compared to the most advanced materials designed for solar absorber applications [51]. Consequently, laser-nanotextured semi-insulating 6H-SiC, following the optimization and customization of process parameters, fulfills the criteria for substantial optical absorptance and elevated spectral selectivity, which are mandatory for obtaining an efficient solar absorbing layers.

4. Conclusions

Single-crystal 6H-SiC, in its semi-insulating form, underwent successful nanotexturing through femtosecond circularly polarized pulsed laser irradiation. The resulting nanostructures exhibit a two-dimensional space arrangement and a spatial periodicity of around 150 nm, fitting the criteria for Highly Spatially Periodic LIPSS (HSFL). Notably, the most regular structures are achieved with the lowest applied pulse energy, approximately 70 μJ corresponding to an energy fluence of 7.3 J cm^{-2}. This was validated using 2D-FFT analysis, revealing distinct bright spots that implies a unique spatial periodicity and a relatively ordered arrangement.

Micro-Raman characterization further confirmed the characteristic peaks of 6H-SiC for the nanostructured samples, without alteration of the structural and compositional phases. However, these peaks exhibited an upshift compared to the reference untreated 6H-SiC peaks, indicative of a significant compressive strain.

Samples treated across their entire surfaces with a single energy pulse of approximately 70 μJ (Φ = 7.3 J cm^{-2}; N = 583) displayed significantly enhanced optical absorption and solar selectivity. Solar absorptance increased from 10 % to 75 %, marking an enhancement of over 7 times compared to the pristine sample. Notably, a maximum selectivity of 2.0, estimated at operating temperatures exceeding 1000 K, underscores the optical effectiveness of laser-nanotextured semi-insulating 6H-SiC. This behaviour makes this surface-modified material as a promising candidate for efficient selective absorption in forthcoming high-temperature solar cells, particularly for integration within concentrated solar energy systems. The outcomes of the present work spotlight the practical utilization potential of laser-nanotextured 6H-SiC induced by LIPSS in advancing solar energy conversion technologies.

CRediT authorship contribution statement

M. Mastellone: Conceptualization, Methodology, Investigation, Visualization, Writing – original draft, Writing – review & editing. **E. Bolli:** Investigation, Visualization. **V. Valentini:** Investigation, Data curation, Visualization. **A. Bellucci:** Conceptualization, Investigation, Validation, Formal analysis, Visualization, Writing – original draft, Writing – review & editing. **S. Orlando:** Methodology, Investigation. **A. Santagata:** Methodology, Investigation. **R. Polini:** Investigation, Data curation, Visualization. **A. Lettino:** Investigation, Data curation, Visualization. **E. Sani:** Investigation, Data curation, Visualization. **D.M. Trucchi:** Formal analysis, Supervision, Writing – review & editing.

Declaration of competing interest

The authors declare that they have no known competing financial interests or personal relationships that could have appeared to influence the work reported in this paper.

Data availability

Data will be made available on request.

Acknowledgements

The authors gratefully acknowledge the administrative collaboration of Dr. Enzo Lucia (CNR-ISM) and Dr. Maria Lucia Pace (CNR-ISM) and the technical support of Mr. Antonello Ranieri (CNR-IC) and of the CNR-ISM technical staff: Mrs. Patrizia Dolce, Mr. Donato Mollica, and Mr. Fabrizio Pallotta.

References

[1] F.A. Müller, C. Kunz, S. Gräf, Bio-inspired functional surfaces based on laser-induced periodic surface structures, Materials 9 (2016) 476, https://doi.org/10.3390/ma9060476.
[2] Y. Lu, Y. Duan, X. Liu, Q. Chen, H.-B. Sun, High-quality rapid laser drilling of transparent hard materials, Opt. Lett. 47 (2022) 921, https://doi.org/10.1364/OL.452530.
[3] L. Wang, Q.-D. Chen, X.-W. Cao, R. Buividas, X. Wang, S. Juodkazis, H.-B. Sun, Plasmonic nano-printing: large-area nanoscale energy deposition for efficient surface texturing, Light Sci. Appl. 6 (2017) e17112, https://doi.org/10.1038/lsa.2017.112.
[4] R.R. Gattass, E. Mazur, Femtosecond laser micromachining in transparent materials, Nat. Photonics. 2 (2008) 219–225, https://doi.org/10.1038/nphoton.2008.47.
[5] D.M. Trucchi, A. Bellucci, M. Girolami, P. Calvani, E. Cappelli, S. Orlando, R. Polini, L. Silvestroni, D. Sciti, A. Kribus, Solar thermionic-thermoelectric generator (ST 2G): concept, materials engineering, and prototype demonstration, Adv. Energy Mater. 8 (2018) 1802310, https://doi.org/10.1002/aenm.201802310.
[6] D. Yao, Z. Hu, R. Zheng, J. Li, L. Wang, X. Yang, W. Lü, H. Xu, Black TiO2-based dual photoanodes boost the efficiency of quantum dot-sensitized solar cells to 11.7%, Nanomaterials 12 (2022) https://doi.org/10.3390/nano12234294.
[7] E. Cappelli, S. Orlando, D. Sciti, A. Bellucci, A. Lettino, D.M. Trucchi, Improving solar radiation absorbance of high refractory sintered ceramics by fs Ti:sapphire laser surface treatment, Appl. Surf. Sci. (2014) 177–183, https://doi.org/10.1016/j.apsusc.2014.01.134.
[8] D. Sciti, D.M. Trucchi, A. Bellucci, S. Orlando, L. Zoli, E. Sani, Effect of surface texturing by femtosecond laser on tantalum carbide ceramics for solar receiver applications, Sol. Energy Mater. Sol. Cells. 161 (2017) 1–6, https://doi.org/10.1016/j.solmat.2016.10.054.
[9] E. Sani, D. Sciti, L. Silvestroni, A. Bellucci, S. Orlando, D.M. Trucchi, Tailoring optical properties of surfaces in wide spectral ranges by multi-scale femtosecond-laser texturing: a case-study for TaB_2 ceramics, Opt. Mater. 109 (2020) 110347, https://doi.org/10.1016/j.optmat.2020.110347.
[10] A. Santagata, M.L. Pace, A. Bellucci, M. Mastellone, E. Bolli, V. Valentini, S. Orlando, E. Sani, S. Failla, D. Sciti, D.M. Trucchi, Enhanced and selective absorption of molybdenum nanostructured surfaces for concentrated solar energy applications, Materials 15 (2022), https://doi.org/10.3390/ma15238333.
[11] J. Bonse, S.V. Kirner, J. Krüger, Laser-Induced Periodic Surface Structures (LIPSS), in: K. Sugioka (Ed.), Handbook of Laser Micro- and Nano-Engineering, Springer International Publishing, Cham, 2021, pp. 879–936, https://doi.org/10.1007/978-3-030-63647-0_17.
[12] J. Huang, K. Xu, J. Hu, D. Yuan, J. Li, J. Qiao, S. Xu, Self-aligned plasmonic lithography for maskless fabrication of large-area long-range ordered 2D nanostructures, Nano Lett 22 (2022) 6223–6228, https://doi.org/10.1021/acs.nanolett.2c01740.
[13] M. Mastellone, A. Bellucci, M. Girolami, V. Serpente, R. Polini, S. Orlando, A. Santagata, E. Sani, F. Hitzel, D.M. Trucchi, Deep-subwavelength 2D periodic surface nanostructures on diamond by double-pulse femtosecond laser irradiation, Nano Lett. 21 (2021) 4477–4483, https://doi.org/10.1021/acs.nanolett.1c01310.
[14] J. Bonse, R. Koter, M. Hartelt, D. Spaltmann, S. Pentzien, S. Höhm, A. Rosenfeld, J. Krüger, Femtosecond laser-induced periodic surface structures on steel and titanium alloy for tribological applications, Appl. Phys. A. 117 (2014) 103–110, https://doi.org/10.1007/s00339-014-8229-2.
[15] S. Arthanari, J.-E. Park, S. Bose, H.W. Kang, S. Kim, M. Yang, H. Lee, J.S. Hwang, Structural color generation on transparent and flexible substrates by nanosecond laser induced periodic surface structures, Adv. Mater. Technol. 8 (2023) 2201725, https://doi.org/10.1002/admt.202201725.
[16] M. Girolami, A. Bellucci, M. Mastellone, S. Orlando, V. Valentini, R.M. Montereali, M.A. Vincenti, R. Polini, D.M. Trucchi, Optical characterization of double-nanotextured black diamond films, Carbon 138 (2018) 384–389, https://doi.org/10.1016/j.carbon.2018.07.055.
[17] J.M. Romano, A. Garcia-Giron, P. Penchev, S. Dimov, Triangular laser-induced submicron textures for functionalising stainless steel surfaces, Appl. Surf. Sci. 440 (2018) 162–169, https://doi.org/10.1016/j.apsusc.2018.01.086.
[18] A.F. Sartori, S. Orlando, A. Bellucci, D.M. Trucchi, S. Abrahami, T. Boehme, T. Hantschel, W. Vandervorst, J.G. Buijnsters, Laser-Induced Periodic Surface Structures (LIPSS) on heavily boron-doped diamond for electrode applications, ACS Appl. Mater. Interfaces 10 (2018) 43236–43251, https://doi.org/10.1021/acsami.8b15951.
[19] S. Amoruso, A. Andreone, A. Bellucci, C. Koral, M. Girolami, M. Mastellone, S. Mou, S. Orlando, G.P. Papari, D. Paparo, R. Polini, A. Rubano, A. Santagata, V. Serpente, V. Valentini, D.M. Trucchi, All-carbon THz components based on

laser-treated diamond, Carbon 163 (2020) 197–201, https://doi.org/10.1016/j.carbon.2020.03.023.
[20] H. Huang, P. Zhang, Z. Yu, X. Zhang, L. Shen, H. Shi, H. Yan, L. Wang, Y. Tian, Effects of periodic surface structures induced by femtosecond laser irradiation on the antibacterial properties of Zr-based amorphous material, Optik 268 (2022) 169760, https://doi.org/10.1016/j.ijleo.2022.169760.
[21] A.H.A. Lutey, L. Gemini, L. Romoli, G. Lazzini, F. Fuso, M. Faucon, R. Kling, Towards laser-textured antibacterial surfaces, Sci. Rep. 8 (2018) 1–10, https://doi.org/10.1038/s41598-018-28454-2.
[22] H.M. Van Driel, J.E. Sipe, J.F. Young, Laser-induced periodic surface structure on solids: a universal phenomenon, Phys. Rev. Lett. 49 (1982) 1955–1958, https://doi.org/10.1103/PhysRevLett.49.1955.
[23] J. Bonse, S. Gräf, Maxwell meets marangoni—a review of theories on laser-induced periodic surface structures, Laser Photon. Rev. 14 (2020) 2000215, https://doi.org/10.1002/lpor.202000215.
[24] M. Mastellone, M.L. Pace, M. Curcio, N. Caggiano, A. De Bonis, R. Teghil, P. Dolce, D. Mollica, S. Orlando, A. Santagata, V. Serpente, A. Bellucci, M. Girolami, R. Polini, D.M. Trucchi, LIPSS applied to wide bandgap semiconductors and dielectrics: assessment and future perspectives, Materials 15 (2022) 1378, https://doi.org/10.3390/ma15041378.
[25] D. Dufft, A. Rosenfeld, S.K. Das, R. Grunwald, J. Bonse, Femtosecond laser-induced periodic surface structures revisited: a comparative study on ZnO, J. Appl. Phys. 105 (2009) 034908, https://doi.org/10.1063/1.3074106.
[26] Y. Yuan, L. Jiang, X. Li, C. Wang, H. Xiao, Y. Lu, H. Tsai, Formation mechanisms of sub-wavelength ripples during femtosecond laser pulse train processing of dielectrics, J. Phys. D 45 (2012) 175301, https://doi.org/10.1088/0022-3727/45/17/175301.
[27] J. Reif, F. Costache, M. Henyk, S.V. Pandelov, Ripples revisited: non-classical morphology at the bottom of femtosecond laser ablation craters in transparent dielectrics, Appl. Surf. Sci. 197–198 (2002) 891–895, https://doi.org/10.1016/S0169-4332(02)00450-6.
[28] Y. Dong, P. Molian, Coulomb explosion-induced formation of highly oriented nanoparticles on thin films of 3C-SiC by the femtosecond pulsed laser, Appl. Phys. Lett. 84 (2004) 10–12, https://doi.org/10.1063/1.1637948.
[29] H. Zhang, J.P. Colombier, C. Li, N. Faure, G. Cheng, R. Stoian, Coherence in ultrafast laser-induced periodic surface structures, Phys. Rev. B 92 (2015) 174109, https://doi.org/10.1103/PhysRevB.92.174109.
[30] A. Rudenko, J.-P. Colombier, S. Höhm, A. Rosenfeld, J. Krüger, J. Bonse, T.E. Itina, Spontaneous periodic ordering on the surface and in the bulk of dielectrics irradiated by ultrafast laser: a shared electromagnetic origin, Sci. Rep. 7 (2017) 12306, https://doi.org/10.1038/s41598-017-12502-4.
[31] A. Bellucci, M. Girolami, M. Mastellone, S. Orlando, R. Polini, A. Santagata, V. Serpente, V. Valentini, D.M. Trucchi, Novel concepts and nanostructured materials for thermionic-based solar and thermal energy converters, Nanotechnology 32 (2021) 024002, https://doi.org/10.1088/1361-6528/abba57.
[32] T. Kimoto, J.A. Cooper, Fundamentals of Silicon Carbide Technology, Wiley, 2014, https://doi.org/10.1002/9781118313534.
[33] S. Mey, C. Caliot, G. Flamant, A. Kribus, Y. Gray, Optimization of high temperature SiC volumetric solar absorber, Energy Procedia 49 (2014) 478–487, https://doi.org/10.1016/j.egypro.2014.03.051.
[34] P.M. Sarro, Silicon carbide as a new MEMS technology, Sensors Actuat. A 82 (2000) 210–218, https://doi.org/10.1016/S0924-4247(99)00335-0.
[35] M. Mastellone, A. Bellucci, M. Girolami, R.M. Montereali, S. Orlando, R. Polini, V. Serpente, E. Sani, V. Valentini, M.A. Vincenti, D.M. Trucchi, Enhanced selective solar absorption of surface nanotextured semi-insulating 6H–SiC, Opt. Mater. 107 (2020) 109967, https://doi.org/10.1016/j.optmat.2020.109967.
[36] J. Chen, X. Xie, Q. Peng, Z. He, W. Hu, Q. Ren, J. Long, Effect of surface roughness on femtosecond laser ablation of 4H-SiC substrates, J. Cent. South Univ. 29 (2022) 3294–3303, https://doi.org/10.1007/s11771-022-5136-0.
[37] Q.Z. Zhao, F. Ciobanu, S. Malzer, L.J. Wang, Enhancement of optical absorption and photocurrent of 6H-SiC by laser surface nanostructuring, Appl. Phys. Lett. 91 (2007) 121107, https://doi.org/10.1063/1.2786863.
[38] J. Song, Y. Dai, W. Tao, M. Gong, G. Ma, Q. Zhao, J. Qiu, Surface birefringence of self-assembly periodic nanostructures induced on 6H-SiC surface by femtosecond laser, Appl. Surf. Sci. 363 (2016) 664–669, https://doi.org/10.1016/j.apsusc.2015.12.096.
[39] T.Q. Jia, F.L. Zhao, M. Huang, H.X. Chen, J.R. Qiu, R.X. Li, Z.Z. Xu, H. Kuroda, Alignment of nanoparticles formed on the surface of 6H-SiC crystals irradiated by two collinear femtosecond laser beams, Appl. Phys. Lett. 88 (2006) 111117, https://doi.org/10.1063/1.2186067.
[40] Z. He, X. Xie, J. Long, T. Liu, Z. Zhang, Q. Lai, Large-area regular periodic surface structures on 4H-SiC induced by defocused femtosecond laser, Semicond. Sci. Technol. 37 (2022) 95005, https://doi.org/10.1088/1361-6641/ac81e6.
[41] C. McDaniel, A. Flanagan, G.M. O' Connor, Evidence for increased incubation parameter in multi-pulse ablation of a Pt:SS alloy using a femtosecond laser at high repetition rates, Appl. Surf. Sci. 295 (2014) 1–7, https://doi.org/10.1016/j.apsusc.2013.12.034.
[42] H. Shimizu, S. Yada, G. Obara, M. Terakawa, Contribution of defect on early stage of LIPSS formation, Opt. Express 22 (2014) 17990–17998, https://doi.org/10.1364/OE.22.017990.
[43] J.M. Liu, Simple technique for measurements of pulsed Gaussian-beam spot sizes, Opt. Lett. 7 (1982) 196–198, https://doi.org/10.1364/OL.7.000196.
[44] L. Porta-Velilla, N. Turan, Á. Cubero, W. Shao, H. Li, G.F. de la Fuente, E. Martínez, Á. Larrea, M. Castro, H. Koralay, Ş. Çavdar, J. Bonse, L.A. Angurel, Highly regular hexagonally-arranged nanostructures on Ni-W alloy tapes upon irradiation with ultrashort UV laser pulses, Nanomaterials 12 (2022), https://doi.org/10.3390/nano12142380.
[45] J. Sládek, K. Hlinomaz, I. Mirza, Y. Levy, T.J.-Y. Derrien, M. Cimrman, S. S. Nagisetty, J. Čermák, T.H. Stuchlíková, J. Stuchlík, N.M. Bulgakova, Highly regular LIPSS on thin molybdenum films: optimization and generic criteria, Materials 16 (2023), https://doi.org/10.3390/ma16072883.
[46] S. Durbach, N. Hampp, Generation of 2D-arrays of anisotropically shaped nanoparticles by nanosecond laser-induced periodic surface patterning, Appl. Surf. Sci. 556 (2021) 149803, https://doi.org/10.1016/j.apsusc.2021.149803.
[47] P.T.B. Shaffer, Refractive index, dispersion, and birefringence of silicon carbide polytypes, Appl. Opt. 10 (1971) 1034, https://doi.org/10.1364/ao.10.001034.
[48] S. Nakashima, H. Harima, Raman investigation of SiC polytypes, Phys. Status Solidi Appl. Res. 162 (1997) 39–64, https://doi.org/10.1002/1521-396X(199707)162:1<39::AID-PSSA39>3.0.CO;2-L.
[49] H.K. Raut, V.A. Ganesh, A.S. Nair, S. Ramakrishna, Anti-reflective coatings: a critical, in-depth review, Energy Environ. Sci. 4 (2011) 3779–3804, https://doi.org/10.1039/C1EE01297E.
[50] C. Kunz, S. Engel, F.A. Müller, S. Gräf, Large-area fabrication of laser-induced periodic surface structures on fused silica using thin gold layers, Nanomaterials 10 (2020) 1–14, https://doi.org/10.3390/nano10061187.
[51] E. Sani, L. Mercatelli, M. Meucci, A. Balbo, L. Silvestroni, D. Sciti, Compositional dependence of optical properties of zirconium, hafnium and tantalum carbides for solar absorber applications, Sol. Energy. 131 (2016) 199–207, https://doi.org/10.1016/j.solener.2016.02.045.